

Structural Optimization Method Towards Synthesis of Small Scale Flexure-based Mobile Grippers

Guo Zhan Lum^{1,2}, Eric Diller^{1,3} and Metin Sitti^{1,4}

Abstract—This paper presents a novel synthesis method for the design of micro-scale robotic flexure mechanisms. A structural optimization method, termed the mechanism-based approach, is used to identify the optimal topology and shape of the flexure mechanisms based on their lump stiffness characteristics. Using several different fitness functions, several optimal flexure designs have been synthesized for use in millimeter-scale mobile grippers (μ -grippers). The stiffness characteristics of the optimal μ -grippers are shown to be better than the thin-beam designs developed using human intuition. Two large-scale prototypes are constructed and experiments are conducted to validate the stiffness analysis. The experimental results are within 20% of the analytical expectations. As a proof of concept, at-scale μ -grippers are constructed based on photolithography and replica molding methods, and demonstrated in simple actuation. The optimal μ -grippers can be applicable for cell manipulations in future works.

I. INTRODUCTION

Mobile micro-robots show promise for non-invasive access to microscale environments for manipulation and interaction with the environment [1]–[3]. Due to their size, these robots have great potential to be employed in many biotech, micro-factory or healthcare applications which require noninvasive access to small spaces [4]–[7]. Some potential applications include utilizing these micro-robots to perform cell manipulation [8], [9], micropart assembly [10], or medical procedures [11]. Previous efforts in remote micro-scale manipulation have involved pushing or fluid-based manipulation [5], [12]. However, these approaches suffer from a lack of precision and 3D manipulation capability for complex part orientation and assembly control. Thus, mobile micro-sized grippers (μ -grippers) that are able to grip and transport other micro-sized objects are the ideal candidates for such applications.

The design for μ -grippers have been demonstrated by Gracias et al., who utilize elastic flat sheets as μ -grippers by activating them via chemical or thermal means. Upon activation, the flat sheets will curl up to entrap/grab the micro-objects [13], [14]. The micro-objects within the μ -grippers can be manipulated effectively by using remote magnetic forces to translate the μ -grippers. Although the response of the μ -grippers are fast, the chemically- or thermally-activated μ -grippers suffer from low actuation precision and in some

cases lack of repeatability. Larger-scale grippers based on the design of compliant mechanisms that can grab micro-objects, are however more common [15]–[17]. As the actuation for these large grippers is delivered via elastic deformation, they can achieve very high precision by eliminating dry friction, backlash and hysteresis [18]–[20]. An additional advantage of using compliant mechanisms is that their sizes are scalable as their designs have ranged from micro- to large-length scales [17]. For example, Kota et al. have designed MEMS flexures based on compliant mechanism design [21]. In order to maximize a compliant mechanism's performance, the ratio of non-actuating to actuating stiffness should be maximized. This is because by having a low actuating stiffness, the intended deflection range for the compliant mechanism can be increased. Likewise, the compliant mechanisms can reduce parasitic motions when they are subjected to external wrenches if they have high non-actuating stiffness.

Based on the Pseudo-Rigid-Body (PRB) method, Shi et al. and Mohamad et al. have designed grippers by replacing the joints of a classical mechanism with compliant joints [22], [23]. Both grippers have high non-actuating stiffness but unfortunately, due to their high actuating stiffness, their workspace of hundreds of microns is small relative to the grippers' size (tens of millimeters). Although the PRB method is a systematic approach for the synthesis of compliant mechanisms, it should be noted that the design of compliant joints is solely based on and potentially limited by human intuition. Thus, the finalized compliant mechanism may not have an optimal non-actuating to actuating stiffness ratio. Another synthesis approach, the structural optimization methods which depend on mathematical programming, has been demonstrated by Sigmund et al. and Wang et al. for the design of compliant mechanisms [17], [24]. Structural optimization methods first discretize the design space into a mesh of identical finite elements where each element in the space is taken as either solid or void. Based on the given fitness function, the state of the finite elements is evolved until an optimum design is obtained. The stiffness characteristics of the compliant mechanisms are determined by finite element analysis (FEA) during the optimization. However, the fitness functions utilized for the grippers designed by Sigmund et al. and Wang et al. are based on a tethered design, where the location of the input and output points are different. Thus, the presented fitness functions and utilized structural optimization algorithm are not applicable for the μ -grippers where the location of their output and input points coincide. This required optimization criteria should be based on the lump stiffness characteristics of the μ -grippers and

¹Department of Mechanical Engineering, Carnegie Mellon University, PA 15213

²School of Mechanical and Aerospace Engineering, Nanyang Technological University, Singapore 639798

³E. Diller is now with the department of Mechanical and Industrial Engineering, University of Toronto, Toronto, M5S 3G8, Canada

⁴Robotics Institute, Carnegie Mellon University, PA 15213

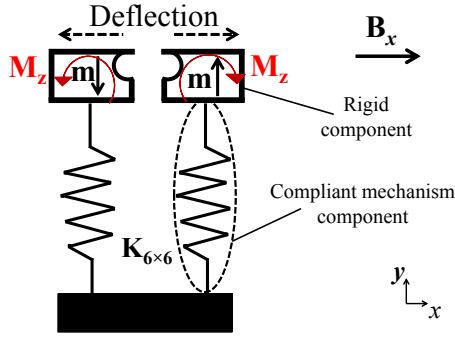


Fig. 1: The conceptual design of the μ -gripper where each side of the gripper has a rigid component and a compliant mechanism component. The rigid component is used to grab micro-objects while the compliant mechanism component is used to provide the desired deflections of the μ -gripper. The rigid components are magnetized along the y -direction and they will experience external \mathbf{M}_z torques when an external x -directional magnetic field, \mathbf{B}_x , is applied. Due to the applied torque, the μ -grippers would ideally have a large deflection in the translational x -direction but small deflection in the rotary z -axis. Furthermore, the μ -grippers should exhibit high stiffness when other external wrenches are applied.

such structural optimization problems in the literature are rare.

This paper presents a novel synthesis method that can synthesize compliant mechanism-based μ -grippers by using the structural optimization method known as the mechanism-based approach [25]. Optimized flexure designs are demonstrated in millimeter length-scale as a proof of concept for micro-scale grippers. The obtained μ -grippers exhibit better lump stiffness characteristics than the human-intuitively designed beam-type counterparts.

II. GRIPPER SYNTHESIS

A. Mechanism-based Approach

The conceptual design of the μ -gripper is shown in Fig. 1, where each arm of the μ -gripper can be analyzed as having a rigid component and a compliant mechanism component. The function of the rigid component is to grab and manipulate micro-objects while the compliant mechanism component allows the μ -gripper to achieve its desired deflections. The rigid component which is located at the gripper tip, is magnetized in the y -axis as shown, and will experience an actuating torque, \mathbf{M}_z , about the z -axis when an external magnetic field in the x -direction (\mathbf{B}_x) is applied. This magnetic torque acts to align the magnetic moment, \mathbf{m} , with the applied field. The ideal characteristics for the compliant mechanism component is to exhibit high compliance in the translation x -axis when it is subjected to \mathbf{M}_z while exhibiting high stiffness for all other wrenches. This implies that the μ -gripper has only 1-DOF, and will reject disturbances for robust object transport. In order to synthesize a μ -gripper that has optimal lump stiffness characteristics, the structural optimization method known as the mechanism-based approach is utilized.

The mechanism-based approach is selected because it has several distinct advantages over other existing structural

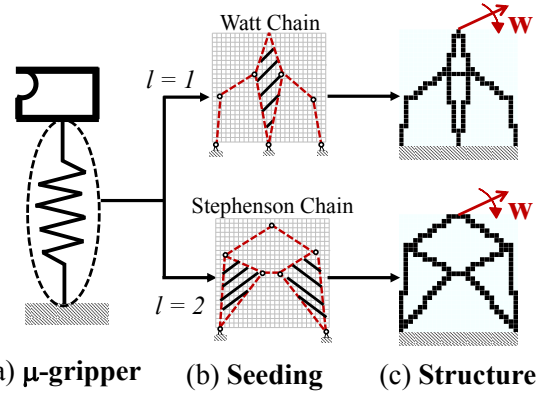


Fig. 2: The seeding process uses either of the two 6-bar linkages, the Watt-Chain or the Stephenson-Chain, to represent the initial topology of the compliant mechanism component, shown in (b). The selection of the seed is dependant on the value of the variable l . Once the seed is selected, it is superimposed onto the discrete design domain where all the finite elements are initially selected as void. The elements which are touched by the seed are converted into solid elements, creating a corresponding structure, shown in (c). The loading point of the structure is indicated by the location where it is subjected to external wrenches, \mathbf{w} .

optimization algorithms such as the SIMP [17], ESO [26] and Level Set Methods [27]. As one major advantage, it eliminates the possibility of having infeasible solutions that contain elements that are neither void nor solid, or disconnected solid elements. Furthermore, as the mechanism-based approach uses Genetic Algorithm (GA) as its solver, it exhibits good convergence. A description for the algorithm is given now in brief, with a more detailed treatment in [25].

The algorithm first discretizes the allowable design space of the compliant mechanism component into a mesh of identical finite elements. The elements in the mesh can only have one of two discrete states, solid or void, and they are all initially selected as void. As seeds to start the GA, two 1-DOF closed-loop traditional mechanisms that have identical kinematic requirement as the μ -gripper are identified by using the Grübler equation [28], which describes the number of Degrees-of-Freedom of a classical mechanism. Two selected classical mechanisms are the commonly-known 6-bar linkages: Watt-Chain and Stephenson-Chain and their topology can be seen in Fig. 2(b). These mechanisms are chosen because they can exist in a symmetrical pose, which is essential for the algorithm to generate symmetrical compliant mechanisms. An advantage of having symmetrical compliant mechanisms is that they can eliminate many parasitic compliances compared with their asymmetrical counterparts. The initial seeds' topology are used as the initial guess for the μ -gripper. As there is more than one possible choice of seed, a discrete design variable, l , is used to select one. The selected seed is then superimposed onto the void design domain, as shown in Fig. 2(b). Elements which came into contact with the seed are converted into solid elements, thus generating corresponding structures as shown in Fig. 2(c). A more detailed description of the selection for the solid elements

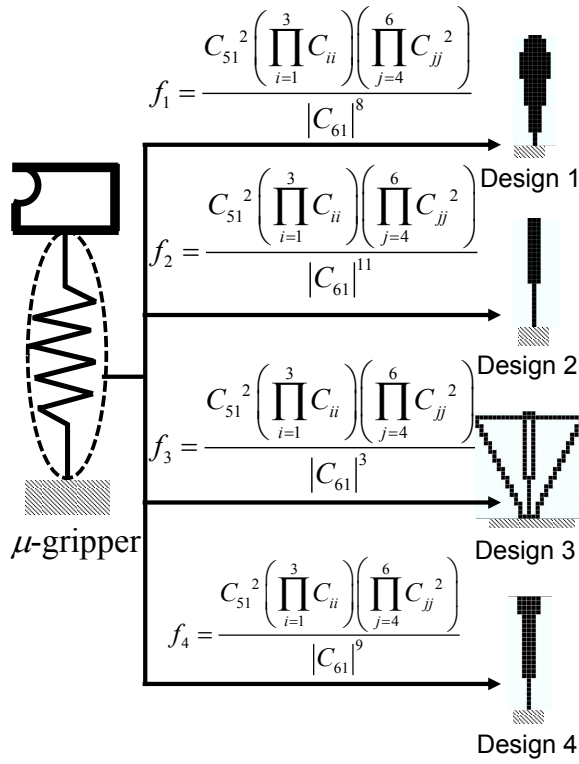


Fig. 3: Several optimal compliant mechanisms are generated with different fitness functions. The numerator of the fitness functions represents the non-actuating stiffness and all the fitness functions have identical numerators. The denominator for each fitness function represents the importance of the actuating compliance. Each optimization uses a population of 100 chromosomes and they converge within 40-60 generations.

can be found in [25]. Different compliant mechanisms can be generated when the seeds' link lengths and orientations vary. The topology of the μ -grippers can also be changed if any link lengths of the seed are reduced to zero. As the position of the links' tip are the design variables, they are encoded in GA's chromosomes. The poses of the seeds are constrained to be symmetrical about the vertical axis located at the centre of the design domain. FEA is used to determine the stiffness characteristics of each chromosome. Based on the stiffness characteristics and the fitness function, each chromosome will be assigned with a corresponding fitness value. The FEA stiffness matrices for each element, \mathbf{K}_e , and the entire compliant mechanism, \mathbf{K}_s , are given as

$$\mathbf{K}_e = \iiint \mathbf{B}^T \mathbf{D} \mathbf{B} dV, \quad \mathbf{K}_s = \sum_{i=1}^{\text{all elements}} \rho_i \mathbf{K}_{e,i}. \quad (1)$$

The matrices \mathbf{B} and \mathbf{D} represent the deformation matrix in FEA and compliance matrix in solid mechanics respectively, while ρ and V present the state and volume of each finite element respectively. If element i is void, ρ_i is 10^{-6} to prevent numerical instability but ρ_i is 1 if the element is solid. Based on the stiffness matrices shown in Eq. (1), the FEA governing equation is

$$\mathbf{K}_s \mathbf{u}_s = \mathbf{f}. \quad (2)$$

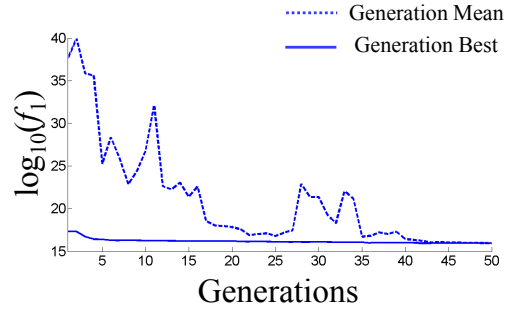


Fig. 4: The log-scale convergence plot for design 1 is used as an example for all the solutions obtained in Fig. 3. All the solutions are able to converge as the fitness values of the generation mean approach the fitness values of the generation best at the end of the optimization process. The typical duration for one optimization process is 4-5 hours.

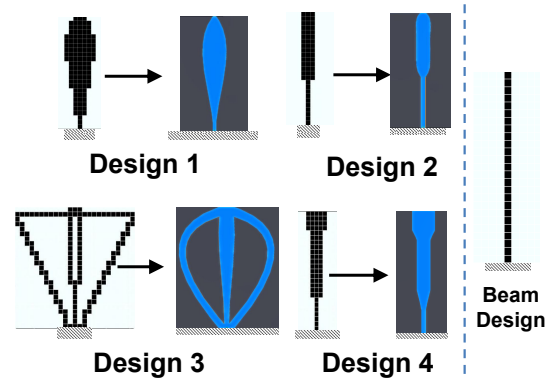


Fig. 5: Smooth splines are used to replace the jagged edges of the compliant mechanism so as to eliminate any potential stress concentration on the fabricated μ -grippers. The intuitively-designed thin-beam flexure is shown on the right.

The vectors \mathbf{u}_s and \mathbf{f} represent the FEA nodal deformations and force loadings on the μ -gripper respectively. The stiffness characteristics of the μ -gripper can be determined by evaluating the rigid-body deflections of the loading point when it is subjected to six orthogonal unit loads, \mathbf{f}_x , \mathbf{f}_y , \mathbf{f}_z , \mathbf{m}_x , \mathbf{m}_y and \mathbf{m}_z . The loadings \mathbf{f}_x , \mathbf{f}_y and \mathbf{f}_z represent the FEA unit force loadings in the x , y and z directions respective, while the loadings \mathbf{m}_x , \mathbf{m}_y and \mathbf{m}_z represent the FEA unit torque loadings about the x , y and z axes respective. The rigid-body deflections of the loading are represented by the 6×6 compliance matrix, $\mathbf{C}_{6 \times 6}$. This matrix can be represented as

$$\mathbf{C}_{6 \times 6} = \mathbf{A} \mathbf{U}_{n \times 6}, \quad \text{where} \quad (3)$$

$$\mathbf{U}_{n \times 6} = \mathbf{K}_s^{-1} [\mathbf{f}_x \quad \mathbf{f}_y \quad \mathbf{f}_z \quad \mathbf{m}_x \quad \mathbf{m}_y \quad \mathbf{m}_z].$$

The six columns of the matrix $\mathbf{U}_{n \times 6}$ correspond to the μ -grippers' FEA nodal deflection when it is subjected to corresponding unit loadings. The rigid-body deflections of the loading point can be obtained by pre-multiplying a matrix \mathbf{A} to $\mathbf{U}_{n \times 6}$. The first three rows of $\mathbf{C}_{6 \times 6}$ represent the trans-

lational deflections while the last three rows represent the rotary deflections. The actuating compliance is represented by C_{61} in $\mathbf{C}_{6 \times 6}$. Fitness functions that maximize the non-actuating to actuating stiffness ratio are used to evolve the compliant mechanism gradually until an optimal solution is determined.

B. The synthesis process

A design domain of $1.25 \text{ mm} \times 1.25 \text{ mm}$ with $50 \text{ }\mu\text{m}$ thickness is chosen for the μ -gripper for ease of fabrication using photolithography and replica molding. The utilized material is a flexible elastomer material (ST-1087, BJB Enterprises), with Young's modulus and Poisson ratio from the literature of 9.8 MPa and 0.45 respectively. The design domain is discretized into a mesh of 25×25 20-node quadratic finite element and each element has edge lengths of $50 \text{ }\mu\text{m}$ resolution due to manufacturing limitation. Several different fitness functions have been implemented to obtain different μ -grippers with different optimal performance. For any chosen fitness function f_i , the optimization problem can be defined as

$$\begin{aligned} & \text{minimize } f_i \\ & \text{subject to: } \mathbf{K}_s \mathbf{u}_s = \mathbf{f}, \end{aligned} \quad (4)$$

where the FEA governing equation is represented by the equality constraint. The obtained optimal compliant mechanisms for four different fitness functions are shown in Fig. 3. The prominent non-actuating compliances for the μ -gripper include the diagonal components in $\mathbf{C}_{6 \times 6}$ and C_{51} . The product of these parasitic compliances form the numerators for all the fitness functions as ideally they should be small. The rotary parasitic compliances, i.e. C_{44} , C_{55} and C_{66} , and C_{51} are regarded as more important for robust gripper operations, thus they have a higher exponential to represent a greater emphasis. The denominator of the fitness functions are different as they have different emphasis on their actuating compliances, C_{61} . Note that fitness functions that have stronger emphasis for their actuating compliances will raise C_{61} to a higher exponential. All the optimization process utilize a population of 100 chromosomes and the optimization process converge within 40-60 generations. The log-scale convergence plot for design 1 is shown as an example in Fig. 4. The required time to perform each optimization process is approximately 4-5 hours. Note that although the obtained design can have more detailed features if the mesh is finer, the required computational time will increase exponentially. Thus, there is a compromise between the selection of mesh and the required computational time to complete the optimization. The jagged edges of the compliant mechanisms are smoothed to eliminate stress concentration and they are compared to thin-beam designs developed via human intuition as shown in Fig. 5. It is noteworthy that the topology of each μ -gripper has been changed during the optimization process. For example, the topologies for designs 1, 2 and 4 have been changed from their original six-bar linkages seeds into a beam with different shapes. Table I compares the compliance matrices of the optimized designs with the

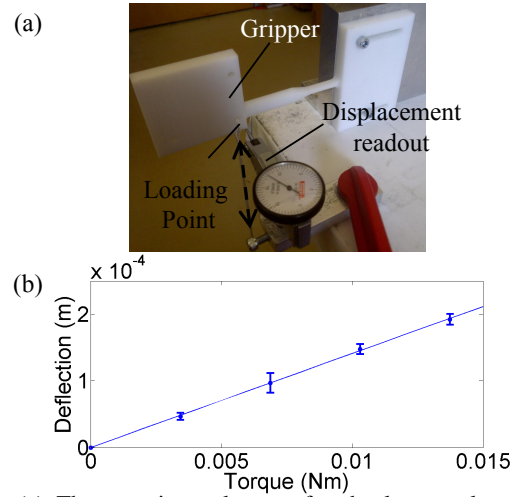


Fig. 6: (a) The experimental setup for the large-scale prototype where the loadings are provided by using calibrated weights. The deflection of the prototype is measured by the dial indicator. By orienting the pose of the prototype, the compliance along different directions of the prototype can be evaluated. (b) Experimental data for the actuating compliance of prototype 1 is shown as an example. The slope of the plot represents the experimental actuating compliance is $-14.1 \times 10^{-3} \text{ m/(Nm)}$ and it agrees with the FEA prediction of $-16.1 \times 10^{-3} \text{ m/(Nm)}$ within 12% deviation. Each datapoint represents the mean from three measurements, and error bars indicate standard deviation.

intuitively-designed beam-type μ -gripper. Here, the width of the intuitively-designed μ -gripper was chosen such that the flexure would have identical actuating compliance for ease of comparison. A more optimal μ -gripper is one that has lower magnitude of C_{ij} in the $\mathbf{C}_{6 \times 6}$. Note that in Table I, $C_{61} < 0$ because when the μ -gripper experiences a positive M_z torque, it will deflect in the negative x -axis direction.

Based on the result listed in Table I, it is apparent that the optimal structures are able to exhibit better stiffness characteristics as they have lower parasitic compliance magnitudes compared with the intuitively designed counterpart. This is especially true for design 1, where eight out of nine components are better and some of the components are approximately two times better.

III. EXPERIMENTS

In order to evaluate the accuracy of the FEA simulation, up-scale prototypes of designs 1 and 2 have been constructed as shown in Table II. Large-scale prototypes are used for ease of deflection and force measurement, which would require μN -level precision for the at-scale prototypes. The utilized material is acetal with Young's modulus and Poisson ratio of 3.1 GPa and 0.45 respectively. Note that the FEA results are applicable for both the μ -grippers and their up-scale counterparts. If the compliances of the prototypes can match their FEA predictions, this indicates that the FEA prediction for the μ -grippers' stiffness characteristics is accurate too.

The experimental setup is shown in Fig. 6(a), using design 2 as an example. Precise loading is induced by hanging calibrated weights, and flexure deflections are measured by a dial gauge indicator. The compliances of the prototype

TABLE I: Compliance matrices comparison between the optimal compliant mechanisms with their intuitively thin beam designs that have identical actuating compliances. Based on the FEA, the optimal μ -grippers have exhibited better stiffness characteristics as most of their components in the $C_{6 \times 6}$ are less than their intuitive designed counterparts. For example, the first design has eight out nine lower parasitic compliances compared to its counterpart.






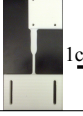
Designs	$C_{6 \times 6}$ of Optimal Structure	$C_{6 \times 6}$ of Beam Design with Identical C_{61}
	$\begin{bmatrix} 19.3 & & & & & \\ 0 & 3.57 \times 10^{-2} & & & & \\ 0 & 0 & 7.81 & & & \\ 0 & -530 & 8.06 \times 10^3 & 1.17 \times 10^7 & & \\ 900 & 0 & 0 & 0 & 1.87 \times 10^7 & \\ -1.71 \times 10^4 & 0 & 0 & 0 & 0 & 1.77 \times 10^7 \end{bmatrix}$ <p style="text-align: center;">SYM</p>	$\begin{bmatrix} 14.0 & & & & & \\ 0 & 6.22 \times 10^{-2} & & & & \\ 0 & 0 & 9.11 & & & \\ 0 & -941 & 1.12 \times 10^4 & 2.00 \times 10^7 & & \\ 1.72 \times 10^3 & 0 & 0 & 0 & 3.55 \times 10^7 & \\ -1.71 \times 10^4 & 0 & 0 & 0 & 0 & 3.04 \times 10^7 \end{bmatrix}$ <p style="text-align: center;">SYM</p>
	$\begin{bmatrix} 46.6 & & & & & \\ 0 & 6.28 \times 10^{-2} & & & & \\ 0 & 0 & 12.8 & & & \\ 0 & -940 & 8.06 \times 10^3 & 1.99 \times 10^7 & & \\ 2.48 \times 10^3 & 0 & 0 & 0 & 5.03 \times 10^7 & \\ -4.75 \times 10^4 & 0 & 0 & 0 & 0 & 5.28 \times 10^7 \end{bmatrix}$ <p style="text-align: center;">SYM</p>	$\begin{bmatrix} 39.8 & & & & & \\ 0 & 8.81 \times 10^{-2} & & & & \\ 0 & 0 & 13.0 & & & \\ 0 & -1.33 \times 10^3 & 1.59 \times 10^4 & 2.84 \times 10^7 & & \\ 1.72 \times 10^3 & 0 & 0 & 0 & 8.06 \times 10^7 & \\ -4.75 \times 10^4 & 0 & 0 & 0 & 0 & 8.47 \times 10^7 \end{bmatrix}$ <p style="text-align: center;">SYM</p>
	$\begin{bmatrix} 11.1 & & & & & \\ 0 & 4.70 \times 10^{-2} & & & & \\ 0 & 0 & 5.60 & & & \\ 0 & -581 & 6.58 \times 10^3 & 1.27 \times 10^7 & & \\ 793 & 0 & 0 & 0 & 1.67 \times 10^7 & \\ -9.86 \times 10^3 & 0 & 0 & 0 & 0 & 1.28 \times 10^7 \end{bmatrix}$ <p style="text-align: center;">SYM</p>	$\begin{bmatrix} 8.04 & & & & & \\ 0 & 5.17 \times 10^{-2} & & & & \\ 0 & 0 & 7.55 & & & \\ 0 & -781 & 9.30 \times 10^3 & 1.66 \times 10^7 & & \\ 1.16 \times 10^3 & 0 & 0 & 0 & 2.39 \times 10^7 & \\ -9.86 \times 10^3 & 0 & 0 & 0 & 0 & 1.77 \times 10^7 \end{bmatrix}$ <p style="text-align: center;">SYM</p>
	$\begin{bmatrix} 37.6 & & & & & \\ 0 & 5.38 \times 10^{-2} & & & & \\ 0 & 0 & 11.3 & & & \\ 0 & -801 & 1.21 \times 10^4 & 1.70 \times 10^7 & & \\ 1.85 \times 10^3 & 0 & 0 & 0 & 3.77 \times 10^7 & \\ -3.63 \times 10^4 & 0 & 0 & 0 & 0 & 3.83 \times 10^7 \end{bmatrix}$ <p style="text-align: center;">SYM</p>	$\begin{bmatrix} 29.4 & & & & & \\ 0 & 7.96 \times 10^{-2} & & & & \\ 0 & 0 & 11.69 & & & \\ 0 & -781 & 1.43 \times 10^4 & 2.57 \times 10^7 & & \\ 3.04 \times 10^3 & 0 & 0 & 0 & 6.28 \times 10^7 & \\ -3.63 \times 10^4 & 0 & 0 & 0 & 0 & 6.27 \times 10^7 \end{bmatrix}$ <p style="text-align: center;">SYM</p>

TABLE II: The predicted FEA compliance of each large-scale prototype are shown in the second column while their corresponding experimental compliances are shown in the last column. The experimental data agrees with the theoretical prediction with a maximum deviation of 20%. The mean deviation for all the experiments is 15%.

	Theoretical $C_{6 \times 6}$	Experimental $C_{6 \times 6}$
Design 1 	$\begin{bmatrix} 0.98 \times 10^{-3} & & & & & \\ 0 & 1.50 \times 10^{-6} & & & & \\ 0 & 0 & 0.434 \times 10^{-3} & & & \\ 0 & 0 & 8.56 \times 10^{-3} & 0.27 & & \\ 0 & 0 & 0 & 0 & 0.402 & \\ -16.1 \times 10^{-3} & 0 & 0 & 0 & 0 & 0.35 \end{bmatrix}$	$\begin{bmatrix} 0.834 \times 10^{-3} & & & & & \\ 0 & 1.85 \times 10^{-6} & & & & \\ 0 & 0 & 0.471 \times 10^{-3} & & & \\ 0 & 0 & 8.40 \times 10^{-3} & 0.335 & & \\ 0 & 0 & 0 & 0 & 0.343 & \\ -14.1 \times 10^{-3} & 0 & 0 & 0 & 0 & 0.423 \end{bmatrix}$
Design 2 	$\begin{bmatrix} 2.00 \times 10^{-3} & & & & & \\ 0 & 2.10 \times 10^{-6} & & & & \\ 0 & 0 & 0.815 \times 10^{-3} & & & \\ 0 & 0 & 16.2 \times 10^{-3} & 0.45 & & \\ 0 & 0 & 0 & 0 & 0.887 & \\ -38.9 \times 10^{-3} & 0 & 0 & 0 & 0 & 0.772 \end{bmatrix}$	$\begin{bmatrix} 2.30 \times 10^{-3} & & & & & \\ 0 & 2.59 \times 10^{-6} & & & & \\ 0 & 0 & 1.01 \times 10^{-3} & & & \\ 0 & 0 & 18.8 \times 10^{-3} & 0.58 & & \\ 0 & 0 & 0 & 0 & 0.752 & \\ -43.5 \times 10^{-3} & 0 & 0 & 0 & 0 & 0.635 \end{bmatrix}$

can be determined experimentally from the slope of their loadings against deflection plots. By changing the orientation of the prototype and the location of the dial, different compliances can be evaluated. Eight compliances, C_{11} , C_{22} , C_{33} , C_{44} , C_{55} , C_{66} , C_{61} and C_{43} for each prototype have been validated. For all evaluated compliances, three sets of data were collected and each set has 5 data points. Fig. 6(b) shows the deflection plot for the actuating compliance of design 1's prototype as an example while the complete experimental data are shown in Table II.

Based on the experimental results, the maximum deviation between the fabricated prototypes' stiffness characteristics and the predicted compliances of FEA is 20%. The mean deviation for all the experiments is 15%. This suggests that the comparison made in Table I is accurate as well.

IV. AT-SCALE GRIPPER FABRICATION

Based on the designs shown in Section II, the μ -grippers have been constructed by using photolithography and replica molding. To fabricate μ -grippers from soft elastomer with

included magnetic particles, a replica molding technique is used which is similar to that seen in [7]. The process includes shape definition by photolithography, replica molding to achieve flexible elastomer gripper shapes, and a magnetization process. The μ -grippers are made from a flexible elastomer material (ST-1087, BJB Enterprises) to allow for larger deflections given the same magnetic actuation. The design requires that each gripper tip be magnetized in opposite directions, which is accomplished at the magnetization step by deforming the μ -gripper arms 90° prior to magnetization. The manufactured μ -grippers are shown in Fig. 7. Fabricated μ -grippers were magnetized and actuated in a magnetic coil system, with results shown in the supplementary video. The actuators are capable of motion on a planar surface and opening/closing actuation in response to large-magnitude fields up to 10 mT in strength.

V. CONCLUSION

In this paper, a novel synthesis method for the design of μ -grippers with optimal lump stiffness characteristics

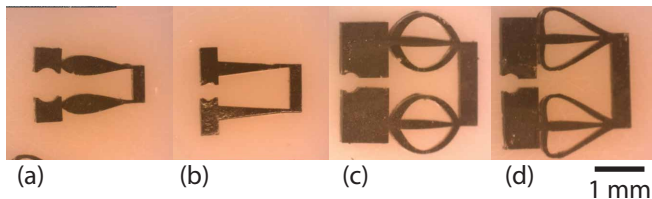


Fig. 7: At-scale fabricated μ -grippers with optimized flexure designs.

based on the structural optimization method, the mechanism-based approach, has been presented. An advantage of using the mechanism-based approach is that it can eliminate the possibility of having disconnected solid elements which can be a prominent issue for optimizing the lump stiffness of a compliant mechanism. This approach first uses two seeds, the 6-bar Watt- and Stephenson-Chains, as an initial guess to represent the topologies of the μ -grippers. Based on the chosen fitness function, the topology of the μ -gripper were gradually evolved to other topologies using GA. The stiffness characteristics of each chromosome were evaluated via FEA. Several fitness functions were utilized to arrive at several optimal compliant mechanisms. Using FEA, the obtained optimal compliant mechanisms were shown to exhibit better stiffness characteristics compared to the intuitively-designed thin beam design with identical actuating compliances. Most of the parasitic compliances for each design were shown to be reduced and some of these parasitic compliances were shown to be approximately two times smaller, representing significant increase in desired μ -gripper characteristics. The low parasitic compliances allow the μ -grippers to execute complicated motions with minimal parasitic motions as shown in the supplementary video. In order to evaluate the accuracy of the FEA comparison, large-scale prototypes were used to verify the stiffness properties to be accurate with at most 20% error. Finally, functional at-scale μ -grippers were constructed for potential micro-scale manipulation applications. Future work will include testing the manipulation performance of the at-scale grippers and analysing the improvement in performance of the optimized flexure designs over the intuitively-designed beam construction. The presented optimization method will also be applied to other micro-scale flexure-based mechanisms where high non-actuating stiffness is of prime importance.

REFERENCES

- [1] M. Sitti, "Miniature devices: Voyage of the microbots," *Nature*, vol. 458, pp. 1121–1122, 2009.
- [2] —, "Microscale and nanoscale robotics systems," *IEEE Robotics and Automation Magazine*, vol. 14, no. 1, pp. 53–60, 2007.
- [3] S. Yim, E. Gultepe, D. Gracias, and M. Sitti, "Biopsy using a magnetic capsule endoscope carrying, releasing, and retrieving untethered microgrippers," *IEEE Transactions on Biomedical Engineering*, vol. 61, no. 2, pp. 513–521, 2014.
- [4] E. Diller, J. Giltinan, and M. Sitti, "Independent control of multiple magnetic microbots in three dimensions," *International Journal of Robotics Research*, vol. 32, no. 5, pp. 614–631, 2013.
- [5] E. Diller, S. Miyashita, and M. Sitti, "Remotely addressable magnetic composite micro-pumps," *RSC Advances*, vol. 2, no. 9, pp. 3850–3856, 2012.
- [6] E. Diller, S. Floyd, C. Pawashe, and M. Sitti, "Control of heterogeneous magnetic micro-robots in two dimensions," *IEEE Transactions on Robotics*, vol. 28, no. 1, pp. 172–182, 2012.
- [7] E. Diller, C. Pawashe, S. Floyd, and M. Sitti, "Assembly and disassembly of magnetic mobile micro-robots towards deterministic 2-d reconfigurable micro-systems," *International Journal of Robotics Research*, vol. 30, no. 14, pp. 1667–1680, 2011.
- [8] T. Kawahara and M. Sugita, "On-chip manipulation and sensing of microorganisms by magnetically driven microtools with a force sensing structure," in *International conference on Robotics and Automation*, Minnesota, USA, 2012, pp. 4112–4117.
- [9] M. Sakar and E. Steager, "Wireless manipulation of single cells using magnetic microtransporters," in *International Conference on Robotics and Automation*, Shanghai, China, 2011, pp. 2668–2673.
- [10] C. Pawashe, S. Floyd, E. Diller, and M. Sitti, "Two-dimensional autonomous micro-particle manipulation strategies for magnetic micro-robots in fluidic environments," *IEEE Transactions on Robotics*, vol. 28, no. 2, pp. 467–477, 2012.
- [11] B. J. Nelson, I. K. Kaliakatsos, and J. J. Abbott, "Microrobots for minimally invasive medicine," *Annual review of biomedical engineering*, vol. 12, no. 1, pp. 55–85, 2010.
- [12] Z. Ye, E. Diller, and M. Sitti, "Micro-manipulation using rotational fluid flows induced by remote magnetic micro-manipulators," *Journal of Applied Physics*, vol. 112, no. 6, 2012.
- [13] A. Azam, K. E. Laflin, M. Jamal, R. Fernandes, and D. H. Gracias, "Self-folding micropatterned polymeric containers," *Biomedical microdevices*, vol. 13, no. 1, pp. 51–8, 2011.
- [14] E. Gultepe, J. S. Randhawa, S. Kadam, S. Yamanaka, F. M. Selaru, E. J. Shin, A. N. Kalloo, and D. H. Gracias, "Biopsy with thermally-responsive untethered microtools," *Advanced materials*, vol. 25, no. 4, pp. 514–9, 2013.
- [15] I. Giouroudi, H. Htzenrofer, J. Kosel, D. Andrijasevic, and W. Brenner, "Development of a microgripping system for handling of micro-components," *Precision Engineering*, vol. 32, no. 2, pp. 148 – 152, 2008.
- [16] N. F. Wang and K. Tai, "Design of grip-and-move manipulators using symmetric path generating compliant mechanisms," *Journal of Mechanical Design*, vol. 130, no. 11, pp. 1 123 051–1 123 059, 2008.
- [17] M. P. Bendse and O. Sigmund, *Topology Optimization: Theory, Methods, and Applications*. Springer, 2003.
- [18] S. T. Smith, *Flexures: Elements of Elastic Mechanisms*. Gordon & Breach, 2000.
- [19] L. L. Howell, *Compliant Mechanisms*. Wiley, 2001.
- [20] Z. Lu, C. Moraes, Y. Zhao, L. You, C. A. Simmons, and Y. Sun, "A micromanipulation system for single cell deposition," in *IEEE International Conference on Robotics and Automation*, Anchorage, Alaska, 2010, pp. 5–10.
- [21] S. Kota, J. Joo, Z. Li, S. Rodgers, and J. Sniogowski, "Design of compliant mechanisms: Applications to mems," *Analog Integrated Circuits and Signal Processing*, vol. 29, no. 1-2, pp. 7–15, 2001.
- [22] X. Shi, W. Chen, J. Zhang, and W. Chen, "Design, modeling, and simulation of a 2-dof microgripper for grasping and rotating of optical fibers," in *IEEE/ASME International Conference on Advanced Intelligent Mechatronics*, Wollongong, Australia, 2013, pp. 1597–1602.
- [23] M. N. M. Zubir and B. Shirinzadeh, "Development of a high precision flexure-based microgripper," *Precision Engineering*, vol. 33, no. 4, pp. 362 – 370, 2009.
- [24] N. F. Wang and K. Tai, "Design of 2-dof compliant mechanisms to form grip-and-move manipulators for 2d workspace," *Journal of Mechanical Design*, vol. 132, no. 3, pp. 0310 071–0310 079, 2010.
- [25] G. Z. Lum, T. J. Teo, G. Yang, S. H. Yeo, and M. Sitti, "A hybrid topological and structural optimization method to design a 3-dof planar motion compliant mechanism," in *IEEE/ASME International Conference on Advance Intelligent Mechatronics*, Wollongong, Australia, 2013, pp. 247–254.
- [26] Y. M. Xie and G. P. Steven, *Evolutionary structural optimization*. Springer, 1997.
- [27] M. Y. Wang, X. Wang, and D. Guo, "A level set method for structural topology optimization," *Computer Methods in Applied Mechanics and Engineering*, vol. 192, no. 1-2, pp. 227–246, 2003.
- [28] C. E. Wilson, J. P. Sadler, and W. J. Michels, *Kinematics and dynamics of machinery*. Pearson Education, 2003.